Trends in Analytical Chemistry 79 (2016) 286–296

Contents lists available at ScienceDirect

Trends in Analytical Chemistry

journal homepage: www.elsevier.com/locate/trac

Recent advances in layer-by-layer strategies for biosensors incorporating metal nanoparticles

Madalina M. Barsan, Christopher M.A. Brett *

Department of Chemistry, Faculty of Sciences and Technology, University of Coimbra, 3004-535 Coimbra, Portugal

ARTICLE INFO

Keywords:
Metal nanoparticles
Metal nanoparticle hybrids
Layer-by-layer
Self-assembly
Biosensor

ABSTRACT

This review focuses on the recent advances in biosensors based on metal nanoparticles (MeNP) incorporated in layer-by-layer (LbL) or self-assembled layers. LbL methodology has been widely used to immobilize biomolecules without affecting their native conformation, and enables at the same time the incorporation of metallic nanomaterials with controlled molecular architecture, in order to improve electronic communication between the biomolecule and the electrode substrate. The methodologies employed for LbL build up will be reported, with depiction of the procedures used to investigate the size, morphology and distribution of the synthesized MeNP. The benefits conveyed by incorporating MeNP into LbL multilayers will be critically examined. Finally, biosensors based on MeNP-LbL architectures will be described and compared, stressing the analytical parameters and applicability to real sample analysis.

Contents

Abbreviations: AChE, acetyl choline esterase; AFM, atomic force microscopy; AgNP, silver nanoparticles; APS, aminopropyl triethylene silane; ATP, 4-aminothiphenol; AuNP, gold nanoparticles; BSA, bovine serum albumin; CBU, cyclic bisureas; chit, chitosan; ChlsOx, cholesterol oxidase; ChOx, choline oxidase; CMM, carbon mesoporous material; CNT, carbon nanotubes; con A, concanavalin A; CTAB, hexadecyltrimethylammonium bromide; CV, cyclic voltammetry; Cys, cysteine; EIS, electrochemical impedance spectroscopy; FTO, fluorine doped tin oxide; G, graphene; GNs, graphene nanosheets; Hb, hemoglobin; HRP, horseradish peroxidase; IL, ionic liquid; ITO, indium tin oxide; k_s, apparent electron transfer rate constant of immobilized species; LOx, lactate oxidase; MeNP, metal nanoparticles; MPA, mercaptopropionic acid; MPTMOS, (3-mercaptopropyl)-trimethoxysilane; PAH, poly(allylamine hydrochloride); PAMAM, polyamidoamine; PB, Prussian blue; PDDA, poly(diallyl dimethylammonium) chloride; PdNP, palladium nanoparticles; PEI, polyethyleneimine; PS, polystyrene; PSS, polystyrene sulfonate; PtNP, platinum nanoparticles; R_{ct}, charge transfer resistance; SEM, scanning electron microscopy; SP1, stable protein 1; TEM, transmission electron microscopy; TvL, Trametes versicolor Laccase.

* Corresponding author: Tel.: +351 239854470; Fax: +351 239827703.
E-mail address: cbrett@ci.uc.pt (C.M.A. Brett).

http://dx.doi.org/10.1016/j.trac.2015.11.019
0165-9936/

1. Introduction

The layer-by-layer (LbL) methodology enables the preparation of structurally well-defined materials, interconnected through weak interactions, such as hydrogen bonding, biospecific recognition, coordination, electrostatic, hydrophobic and dipole–dipole interactions. The methodology is especially valuable for the immobilization of enzymes, since it enables the preservation of their native structure and activity. Therefore, an increasing number of LbL architectures, with precise control of the composition and film thickness at the molecular level, are being developed for use in new bioanalytical devices [1]. The molecular organisation resulting from the self-assembly process should lead to more efficient sensor platforms as well as requiring smaller quantities of the chemical and biological modifier components than in conventional sensor construction.

The build-up of LbL structures on solid substrates requires the presence of a functional group, usually introduced by deposition of a self-assembled monolayer (SAM), which is a highly organized adsorbed layer. SAM can be formed by chemisorption of amphiphilic organic molecules, containing groups such as thiols, disulphides, amines, acids or silanes [2,3], on top of which LbL assemblies are easily constructed by electrostatic attraction, with precise control of their properties by carefully choosing the configuration, type of polyelectrolytes, number of layers, etc. Moreover, the use of nanomaterials in such LbL architectures, such as metal nanoparticles, carbon nanotubes, graphene etc., has been shown to increase the electronic conductivity and improve the communication between the immobilized biomolecule and the electrode surface. Among the nanoscale materials, metal nanoparticles (MeNP) have been extensively used to improve LbL biosensor performance, especially noble metal nanoparticles (NP), e.g. AuNP, AgNP, PtNP and PdNP, since they possess high stability, conductivity, biocompatibility and size-related electronic, magnetic and optical properties [4]. Beside noble metal NP, iron and iron-oxide magnetic NP have been widely employed in electrochemical biosensors, offering the same advantages as the noble NP such as an increase in enzymatic enzyme apparent activity and reduction of the difficulties associated with mass transfer, but with lower cost and easier preparation [5]. A new trend is the adsorption of metal nanoparticles on porous micro-capsules of controllable size, which can be synthesized using a combination of polyelectrolytes [6,7]. Other nanoparticles used in LbL biosensors are titanium nitride (TiN_NP), MnO_2 and ZnO_NP.

The overall performance of the biosensor is directly influenced by the MeNP size, distribution and immobilization/dispersion, the first of these being controllable by the synthesis protocol. Chemical techniques are by far the most used for MeNP synthesis, usually involving the reduction of the noble metal ion by chemical reducing agents, such as sodium borohydride, sodium citrate, etc. The MeNP synthesised chemically are very unstable and prone to form aggregates, thus requiring the addition of a stabilizer, which can functionalize the MeNP at the same time, facilitating their use in LbL assemblies and/or their dispersion in organic/inorganic media [8]. In general, chemical synthesis has little control on the MeNP size, electrochemical and photochemical techniques emerging as a new alternative since they allow precise control of the particle size, morphology and density, by controlling the deposition parameters, such as the applied potential, the pulse time for both nucleation and growth processes, etc. [9–12].

The aim of this review is to examine the ways in which electrochemical and optical biosensors incorporating MeNP, constructed using the LbL technique, have evolved during the past 5 years (2010–2015). The methodology behind the MeNP_LbL assemblies will be discussed, focussing on the functionalization of MeNP, and the influence of the metal nanoparticles employed on the overall performance of the biosensor. The strategies used to explore the MeNP size, distribution and morphology will be presented, with emphasis on the structure of hybrid materials containing MeNP. Finally, the analytical performance of the biosensors developed using the MeNP are discussed, including electrochemical biosensors based on enzymes, protein, DNA/RNA and aptamers, and optical biosensors.

2. Methodology for the self assembly of metal nanoparticles

The methodologies employed in LbL self-assembly containing metal nanoparticles, have usually involved thiolated compounds, or amino-terminated compounds including PAMAM dendrimer, chitosan etc., and are exemplified in Schemes 1 and 2. Commonly used precursors for synthesizing noble metal MeNP are chloroauric acid ($HAuCl_4$), hexachloroplatinic acid (H_2PtCl_6), potassium tetrachloroplatinate or tetrachloropalladate (K_2PtCl_4, K_2PdCl_4), and for the chemical reduction the most used are sodium citrate and borohydride, hydrazine, hydrogen, and ascorbic acid. These will now be surveyed in more detail.

2.1. Procedures based on thiolated compounds

Thiolated sol gels were extensively used for enabling the self-assembly of AuNP in different electrode architectures, and is illustrated in Scheme 1. A self-assembled monolayer of 3-mercaptopropyltrimethoxysilane (MPTMOS) on ITO was modified with adsorbed AuNP using two methods: 1) pre-concentration of copper followed by its galvanic replacement with Au or 2) chemical adsorption of AuNP through the thiolate (-SH) terminal functionality from the monolayer, to obtain ITO/MPTMOS-$AuNP_{1,2}$ [13], the latter also being used in [14,15]. In [15], a Pt electrode modified with MPTMOS, containing CNT and ChOx, was immersed in AuNP and used as substrate for stepwise deposition of oppositely charged $PDDA^+$ and $AChE^-$ to get the final biosensor Pt/MPTMOS(CNT_$PDDA^+$+$ChOx^-$+$AuNP^-$)/{$PDDA^+$/$AChE^-$}$_n$. The sol gel network entrapped the CNT and ChOx and the –SH of the sol-gel enabled covalent attachment of AuNP. In other work, a GCE/G modified with ZnO dispersed in a sol-gel of aminopropyl triethylene silane (APS), served to anchor AuNP in order to obtain GCE/G/TiO_2/AuNP [16].

Other thiolated compounds were also used for the self-assembly of AuNP. A hybrid material of graphene nanosheets_AuNP (GNs_AuNP) was obtained using sulfur-modified GNs, which was able to bind gold ion precursors from the solution phase onto the GNs, these being reduced by an Ar/H_2 stream to form GNs_AuNP hybrids. A film of GNs_AuNP hybrid was then deposited on GCE using

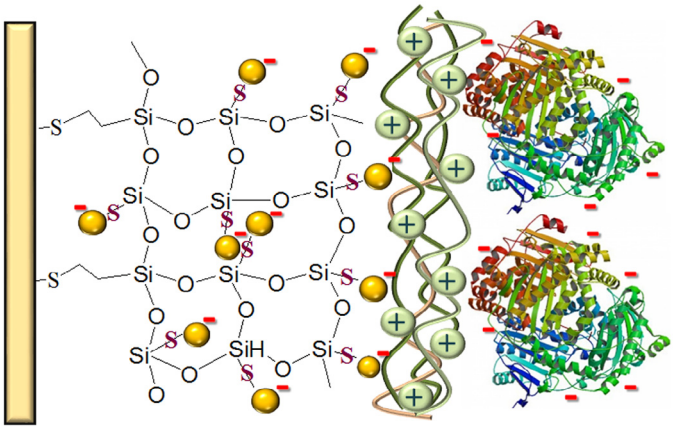

Scheme 1. Schematic representation of self-assembly of thiolated sol-gel, AuNP, cationic polymer and enzyme.

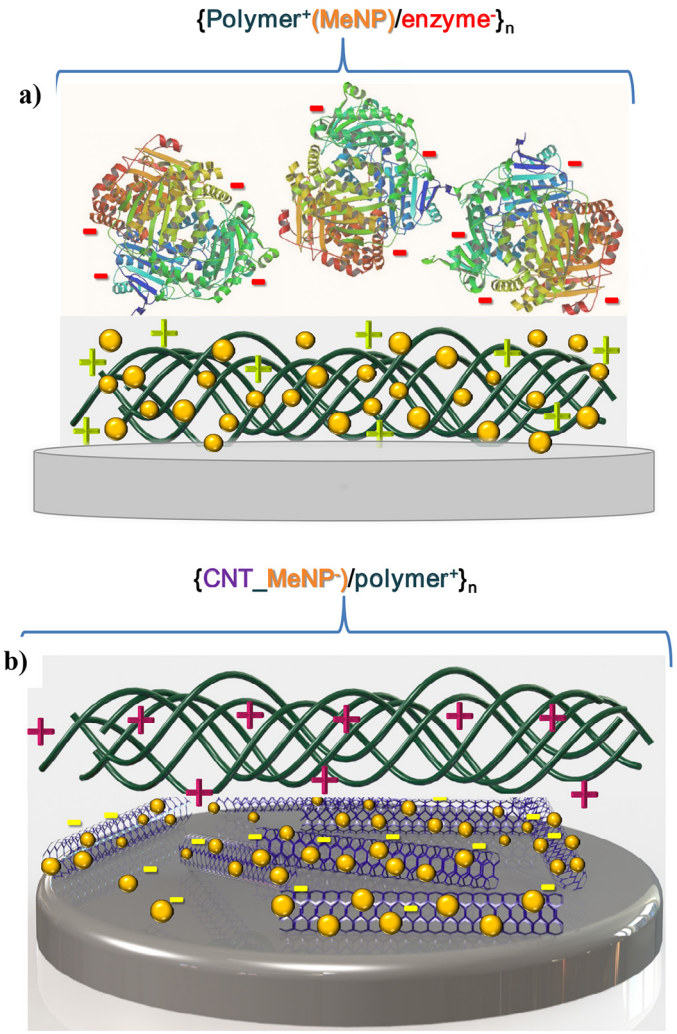

Scheme 2. Schematic representation of LbL assemblies of a) {polymer(MeNP)/enzyme}$_n$ and b){CNT_MeNP/polymer}$_n$.

4-aminothiphenol (ATP) to form GCE/ATP/GNs_AuNP, the amino groups binding to the negative surface of GCE and the thiol to the AuNP [17]. In [18], in order to incorporate AuNP, stable protein 1 (SP1), which has a highly stable ring shape, was modified with cysteine in its inner part, and surrounded by 12 attached GOx monomers. Multiple LbL were deposited based on SP1's capacity to self-assemble into three-dimensional nanostructures, to finally obtain the biosensor {GOx-Cys- SP1-AuNP}$_8$. AuNP decorated CNT were immobilized on ITO by using mercaptopyridin (MPy) as a linker for AuNP to obtain ITO/MpY/CNT_AuNP [19]. Mercapto propionic acid (MPA) was chemisorbed on Au electrode, followed by the assembly of a composite comprising cyclic bisureas (CBU) and AuNP and the covalent attachment of HRP. Due to the chemical and steric structure of the CBU, they ensure the immobilization of the enzyme through hydrogen bonding, therefore CBU/AuNP hybrids were fabricated, as to increase the electron transfer efficiency through the composite [20]. Negatively charged AuNP were obtained using 3-mercaptopropionic acid and 11-mercaptoundecanoic acid, to get AuNP-COOH. An Au electrode modified with chemically adsorbed cysteamine is linked to AuNP-COOH through EDC/NHS, then modified further with fullerenols via ester bonds with EDC/NHS; finally the enzyme is attached to the fullerenols through the same ester bonding in the presence of EDC/NHS [21]. An IL-CPE was fabricated using 1-butylpyridinium hexafluorophosphate ($BPPF_6$) binder and graphite powder and AuNP were electrodeposited on the surface of the IL-CPE. Mercaptoacetic acid (MAA) was then self-assembled on the IL-CPE/AuNP, which served to cross-link the ssDNA probe using EDC/NHS [22]. Cysteine coated Fe_3O_4_NP were immobilized on SAM of carboxylated MBA through EDC and NHS [23].

2.2. Procedures based on amino-terminated compounds

Amino moieties have also been crucial in enabling the self-assembly of metal nanoparticles, and include amino-functionalized CNT, amino-terminated ionic liquid, thionine, poly(allylamine hydrochloride) (PAH), polyaniline (PANI), hexadecyltrimethylammonium bromide (CTAB), the dendrimer PAMAM and the natural polymer chitosan.

A hybrid nanocomposite of G_TiO_2 was used as supporting material for the reduction and dispersion of PdNP, photo-generated electrons from UV-irradiated TiO_2 reducing Pd^{2+} to PdNP. LbL assembly was then performed by dipping a negatively charged GCE^- into a dispersion of amino-functionalized CNT (CNT-NH_3^+), followed by adsorption of negatively charged G/TiO_2–Pd. For immobilizing GOx^-, an additional layer of CNT-NH_3^+ was added to obtain GCE^-/{CNT-$NH^+{}_3$/(G/TiO_2–$Pd)^-$}$_n$/CNT-NH_3^+/GOx^-/Nafion [24]. GCE coated with TiN_NP was modified with 1-(3-aminopropyl)-3-,methylimidazolium bromide, an amino terminated ionic liquid (IL-NH_2) by potential cycling electro-oxidation of the amine group; multilayer films were then formed based on electrostatic interaction between IL with positive charge and negatively charged catalase [25].

Self-assembled multilayers of Nafion, thionine (TH) and PdNP were successfully prepared. $Nafion^-$ was firstly dropped on to a bare GCE, which enabled TH^+ adsorption through electrostatic interaction, on top of which PdNP were adsorbed by using the amino group of TH as linker [26]. In [6], the fabrication of AuNP-assembled capsules (AuNP_C) was possible by using spherical aggregates as substrate, fabricated using HPO_4^{2-} anions and the cationic polyelectrolyte PAH^+, on which AuNP were adsorbed by electrostatic interaction. The nanoporous structure allows the adsorption of proteins, such as hemoglobin (Hb). By controlling the ratio of total negative charges to the total positive, capsules of different sizes are obtained [6]. Similarly, PS/$PANI^+$ capsules served as core-shells for the deposition of AuNP, which were synthesized by chemical oxidation, polymerized PANI shell and fibres being formed on the PS template. The configuration changes of the PANI chains resulting from the doping/dedoping procedure led to various loading amounts of AuNP, held on the surface of the PS/PANI composite microspheres via the coordination bond between the nitrogen electron lone pair on the PANI backbone and $AuCl_4^-$ ions, followed by their chemical reduction [7].

PAMAM dendrimer was successful for the self-assembly of PtNP and AuNP. PtNP-PAMAM and CNT were covalently coupled by 1-ethyl-3-[3-(dimethylamino)propyl] carbodiimide (EDC) to form PtNP-PAMAM/CNT, which served to anchor the negatively charged GOx^- to obtain ITO/{(PtNP-PAMAM/CNT)$^+$/GOx^-}$_n$ [27]. Positively-charged dendrimer AuNP, AuNP-PAMAM, and negatively charged CNT, led to GCE/{CNT^-/(PAMAM-AuNP)$^+$}$_n$ which was then used to immobilize negatively-charged AChE [28].

Chitosan has been used as polycation for LbL assembly, since the amino groups are positively charged at acidic pH. It was successfully used for the dispersion of nanomaterials in LbL structures, carbon and metallic, including CNT and graphene [29,30]. A PtNP_CNT nanocomposite, dispersed in positively-charged chitosan was dropped onto GCE and used as substrate for the LbL deposition of concanavalin A (conA) and GOx, based on biospecific affinity, to obtain GCE/chit$^+$(CNT-PtNP)/{conA/GOx}$_3$ [31]. Core-shell nanoparticles of Fe_3O_4 covered with Pt (Fe_3O_4@PtNP) were used to

fabricate a LbL biosensor containing Hb, chitosan being used as a precursor, to finally obtain GCE/chit$^+$/{Fe_3O_4@PtNP$^-$/Hb$^+$}$_n$ [32].

The polycation PDDA$^+$ has been mainly used for the functionalization of materials, so as to introduce a positive charge on the substrate surface and enable its use in LbL assemblies. For example, in [33], PDDA$^+$ was first attached to carbon mesoporous material (CMM) and PtNP was then attached via electrostatic interaction to give PDDA$^+$(CMM-PtNP). GCE was then modified with this PDDA$^+$(CMM-PtNP) and the enzymes GOx and LOx were immobilized on top.

A hybrid material of TiO_2_CNT was dispersed into positively charged chitosan on top of which negatively charged Prussian blue was deposited to obtain GCE/chit$^+$(TiO_2_CNT)/PB$^-$. PDDA$^+$ functionalized AuNP, was then adsorbed onto the PB film, followed by deposition of negatively charged GOx to obtain the final biosensor GCE/chit$^+$(TiO_2_CNT)/PB$^-$/PDDA$^+$_AuNP/GOx$^-$ [34]. TiO_2–G was dispersed PDDA$^+$ and used as matrix for the electrochemical deposition of Pt and Pd NP. To enable the adsorption of negatively charged enzymes, another layer of PDDA$^+$(TiO_2–G) was added [35]. A novel CNT$^-$/PDDA$^+$/PtNP$^-$/DNAzyme bioconjugate was prepared via LbL assembly of PtNP and PDDA polyelectrolyte on carboxylated CNT, followed by functionalization with DNAzyme and reporter probe DNA through platinum-sulfur bonding [36]. Similarly, poly(allylamine hydrochloride) (PAH$^+$), was used to wrap AuNP decorated CNT as to electrostatically interact with negatively charged enzymes, enabling the formation of multilayers of {PAH$^+$(CNT–AuNP)/HRP$^-$}$_m$ and {PAH$^+$(CNT–AuNP)/ChlsOx$^-$}$_n$ [37]. In other cases, the PDDA was used alone as a polycation together with polyanaions such as PAS$^-$, PSS$^-$. A screen printed carbon electrode modified with MnO_2_NP was used as substrate for the LbL assembly of {PDDA$^+$/PAS$^-$}$_2$ and {PDDA$^+$/ChOx$^-$}$_3$ [38]. Horseradish peroxidase (HRP) was assembled on the Fe_3O_4_NP via LbL using PSS$^-$ and PDDA$^+$ as to form Fe_3O_4_NP/PSS$^-$/PDDA$^+$/HRP$^-$. Signal probe and diluting probe were then immobilized on the Fe_3O_4_NP-HRP through the AuNP bridge to obtain Fe_3O_4_NP-HRP/AuNP/DNA bioconjugates [39]. CNT modified with PSS$^-$ were assembled together with PDDA$^+$, on top of which AgNP were electrochemically deposited by a potentiostatic nucleation pulse plus growth pulse, to form ITO/{CNT-PSS$^-$/PDDA$^+$}$_6$/AgNP [12].

3. Strategies for identification of the synthesized MeNP and MeNP hybrid materials

The techniques most used to investigate electrode surfaces modified with metal nanoparticles and the steps in the formation process of hybrid-based metal nanoparticles have been scanning electron microscopy (SEM), transmission electron microscopy (TEM) and atomic force microscopy (AFM). Others were X-ray diffraction (XRD), UV-vis, high resolution TEM (HRTEM), X-ray photoelectron spectroscopy (XPS), selected area electron diffraction (SAED) and energy-dispersive X-ray spectroscopy (EDX).

The adsorption of Fe_3O_4_NP on electrode substrates is visible in AFM images, the nanoparticles having a diameter of ~15 nm [23]. SEM images confirmed the self-assembly of 20 nm TiN_NP on an amino-terminated ionic liquid, previously deposited on the electrode surface [25]. TEM images revealed the importance of using acetate-based MnO_2 nanoparticles, which had wrinkled lamellar structures with estimated thickness 0.3–0.6 nm and characteristic dimensions of 50–120 nm, being considerably smaller than the chloride-based ones [38]. TEM images indicated that 14-15 nm AuNP were almost spherical in shape [15,40], as exemplified in Fig. 1a [40], and SEM images show that they can be located inside and outside a MPTMOS sol-gel network [15] or covering graphene, see Fig. 1b [40].

An increase in particle size was indicative of successful modification of, or by, metal nanoparticles. By scanning tunneling microscopy (STM) it was possible to see an increase in AuNP

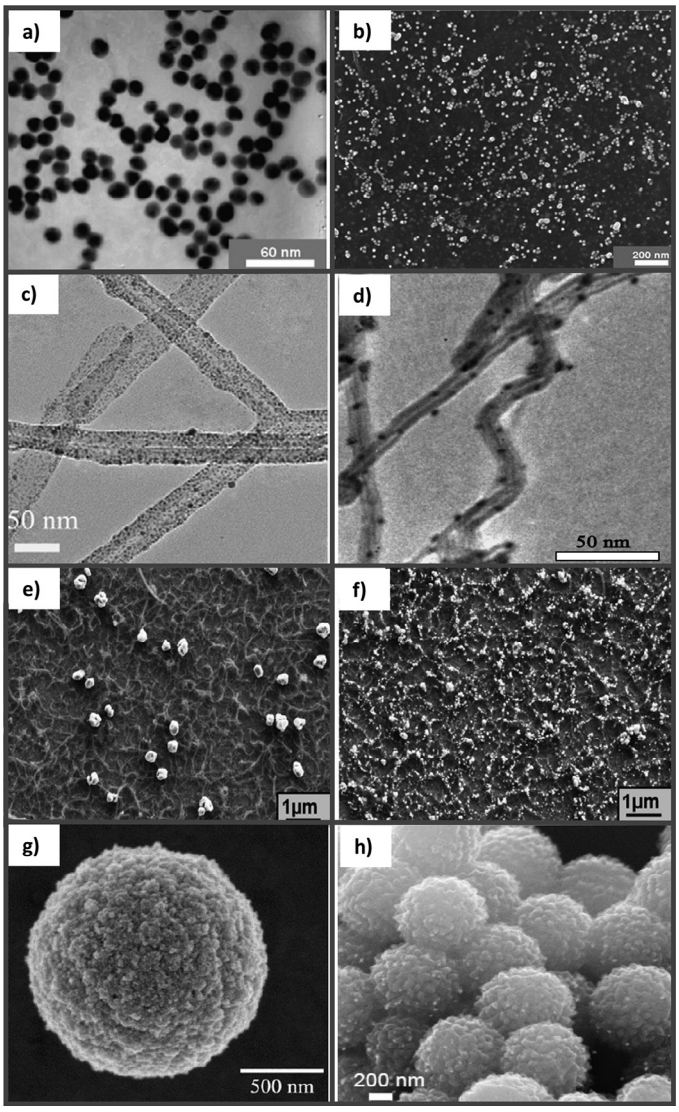

Fig. 1. a) TEM of AuNP and b) SEM images of AuNP adsorbed on graphene [40], c) and d) TEM images of PtNP on CNT [31,36],e) and f) Ag nanoclusters deposited on {PDDA/CNT}$_6$ for different nucleation/growth conditions [12], SEM of AuNP adsorbed on microspheres of g) HPO_4^{2-}/PAH [6], and h) PS/PANI [7]. All micrographs reproduced with permission of the copyright owners.

diameter due to fullerenol attachment through mercaptoundecanoic acid [21]. Similarly, the size of PAMAM-AuNP is about 13 nm and that of the AuNP in the dendrimer complex is about 8 nm, identified in SEM images [28]. AFM images revealed an increase in Fe_3O_4 size after PtNP coating, from 10 to 25 nm, with XPS results revealing the coexistence of Fe^{III} and Pt^0 [32]. The successful PDDA wrapping of AuNP was seen in TEM and SEM images by their increase in size after interacting with PDDA [34]. The average sizes of Fe_3O_4_NP, AuNP, and AuNP–HRP– Fe_3O_4_NP conjugates were 10 nm, 5 nm and 35 nm in diameter, proving successful LbL assembly [39].

The formation of metal nanoparticle hybrid materials was investigated by using several techniques. AuNP-graphene nanosheet hybrids were observed by XRD, which revealed an ordered crystal structure of GN with new diffraction peaks characteristic of the face-centred-cubic crystallographic structure of Au. XPS analysis allowed the identification of elemental Au^0 and Au^+, the latter present due to the formation of Au-S bonds. Also, HRTEM analysis show a homogeneous distribution of AuNP on the GN surface with an average particle size of 6 to 8 nm [17]. Another hybrid material based on

TiO_2 and PdNP was seen by TEM, with irregular spherical and rod-like morphologies of TiO_2 of high crystallinity, and a new visible spherical structure of 5 nm diameter attributed to PdNP [24]. AuNP of similar size were loaded on the surface of the PS/PANI microspheres, seen in SEM images; XRD analysis confirmed the loading of AuNP onto the microspheres and XPS identified the presence of elemental gold [7]. SEM images of AuNP showed that they were embedded in the porous structure of G and ZnO-G [16,40], as clearly seen in Fig. 1b [40]. Similarly, it was possible to see by TEM that 5 nm PtNP can be uniformly dispersed in a mesoporous carbon (MC) matrix. Images of MC modified with different PtNP loadings from 5 to 50% allowed choosing the best loadings of 20-30%, which had an increased NP density with no aggregation [33].

When MeNP are deposited on CNT, they are usually dispersed along the surface of the nanotubes, as can be seen in the TEM images in Fig. 1c and d. TEM images revealed highly dispersed PtNP on the sidewall of the CNT with no aggregation [27,31,36], as shown in Fig. 1c [31,36]. SEM images of a 4-bilayer structure containing CNT and AuNP showed that AuNP were uniformly dispersed on CNT surfaces without any visible aggregation [37]. The structures of AgNP electro-deposited on CNT can be controlled by using the nucleation and growth technique: AgNP increased in size progressively with the growth time from 270, to 315 and 425 nm while with increase in nucleation time, their density increased and the size decreased to 20 nm. AgNP exist mostly along the length of the CNT, since the negatively-charged functional groups of CNT, due to PSS^- modification, attract positively charged silver ions from the solution, to begin the nucleation, as seen in Fig. 1e and f [12].

SEM images of ZnO, ZnO/AuNP and AuNP deposited on CNT show that CNT are covered with a porous ZnO film, confirmed by Raman analysis. The morphology became rougher after AuNP deposition due to the ZnO being fully covered with AuNP of 10 nm diameter. The direct electrodeposition of AuNP onto CNT, without the ZnO film precursor, leads to the formation of large AuNP of 150 nm diameter, with the occurrence of aggregation, the ZnO having the key role of facilitating the deposition of well-distributed, dense and small gold nanoparticles onto the substrate [41].

When MeNP are adsorbed on pre-synthesized microspheres, they usually cover their entire surface, as depicted in Fig. 1g, when AuNP cover a HPO_4^{2-}/PAH^+ capsule [6] and in h) a $PS/PANI^+$ [7].

The variation in surface roughness, observed in AFM images, upon modification with nanoparticles was also indicative of surface modification, the increase in surface roughness occurring usually after MeNP modification [39,42]. An increase in roughness was observed when TiO_2-G was modified with Pt_PdNP, the alloy NP being deposited on the peaks sticking out of the material, while the deposition of AuNP smoothed the surface, since they occupied the valleys between the peaks of TiO_2-G/Pt_PdNP [35]. The AuNP height seen in AFM images was 2 nm, while that of a single monolayer of the GOx-Cys-SP1/AuNP was 8 nm, corresponding to the 6 nm high GOx-Cys-SP1 plus 2 nm AuNP [18].

UV-vis was also useful for identifying the adsorption of AuNP [6,15,34]. When assembled onto pre-synthesized PAH capsules, the typical adsorption was redshifted, which also happened when Hb were adsorbed onto AuNP [6].

4. The role of metal nanoparticles and metal nanoparticle hybrids

Metal nanoparticles, like other nanostructured materials, provide a suitable micro-environment for the immobilization of proteins, especially enzymes, maintaining their bioactivity. Their presence in a layer-by-layer assembly can be crucial for enabling electronic communication between the redox centre of proteins and the electrode substrate [43], since electron transfer can often be hindered due to increasing numbers of bilayers and the presence of insulating materials.

A standard redox couple, for example hexacyanoferrate(III)/hexacyanoferrate(II), is often used to access the electrochemical properties of a modified electrode by employing electrochemical techniques such as cyclic voltammetry (CV) and/or electrochemical impedance spectroscopy (EIS). The incorporation of MeNP into LbL structures leads to an increase in both hexacyanoferrate redox peaks, usually due to an increase in surface area and/or increase in electronic conductivity inside the LbL structure (which can contain less conductive polymers/films or proteins), with a decrease in peak-to peak separation, reflecting faster kinetics at the MeNP modified electrode, similar to the effect of carbon nanomaterials incorporated in LbL structures [44].

Such behaviour was observed at $FTO/\{BSA\text{-}G^+/AuNP^-\}_5$ [40], GCE-ATP-GNs-AuNP, where AuNP-graphene nanosheets (GNs) hybrids increased the redox peak current by a factor of 3, unlike the GNs or AuNP used alone, this being ascribed to the hybridization of GNs with AuNP [17]. The deposition of a first layer of Fe_3O_4@PtNP had the same effect, while incorporation of Hb, and further bilayers in $GCE/chit^+/\{Fe_3O_4@PtNP^-/Hb^+\}_n$ led to a decrease of I_p and an increase of ΔE_p, due to the insulating nature of the protein [32]. TiO_2–G hybrid incorporated in $GCE/PDDA^+(TiO_2\text{-}G)/Pt\_PdNP/PDDA^+(TiO_2\text{-}G)/AuNP$ decreased the redox peaks due to TiO_2, and metallic nanoparticles, both Pt_PdNP alloy and AuNP, significantly increased the peak currents [35]. An increase in peak current upon MeNP incorporation was also observed at $GCE/(PDDA^+\text{-}CMM)/PtNP$ [33], at Au modified with mercaptobenzoic acid Fe_3O_4_NP [23], ionic liquid carbon pate electrode (IL-CPE)/AuNP [22] and $FTO\{G/AuNP\}_n$ [40].

Electrochemical impedance spectra recorded in the presence of a redox probe can give information about the electronic conductivity of the modified electrode. In this case, the monitoring of the charge transfer resistance (R_{ct}), used to fit the high frequency semicircle part of a Nyquist plot, enables the effect of the modification of the electrode substrates to be seen. The incorporation of nanoparticles leads to a decrease of R_{ct}, observed for AuNP-GNs hybrids [17], CNT–AuNP in $Au\text{-}MPS^-/PAH^+/PSS^-/\{PAH^+(CNT–AuNP)\}_n$ [37], AuNP in MPTMOS sol-gel [14], and in IL_CPE [22], and Fe_3O_4_NP on a mercaptobenzoic acid modified Au electrode [23]. A first layer containing Fe_3O_4@PtNP also decreased the R_{ct} value, but further numbers of bilayers increased it due to the presence of insulating hemoglobin [32], similar to what was observed in the case of myoglobin incorporation into LbL [45]. The R_{ct} value of an unmodified Pt electrode increased upon modification with MPTMOS(CNT-$PDDA^+$+ChOx), the sol–gel acting as the inert electron and mass transfer blocking layer, and decreased when AuNP are chemisorbed, implying that AuNP acted as good electron conducting material [15].

A decrease in R_{ct} can also be observed without any redox probe, when the modified electrode contains redox active polymer, protein etc. This was the case of Hb-modified electrodes, when it was observed that both G-ZnO and AuNP increased electronic communication between Hb and the electrode substrate [16]. Similarly, spectra recorded in the presence of glucose at $ITO/\{(PtNP\text{-}PAMAM/CNT)^+/GOx^-\}_3$ and two others, one without CNT and the other without PtNP, showed that the electrode containing both CNT and PtNP had a lower R_{ct}, due to higher electron conduction pathways and synergistic effect [27].

In other cases, the advantage in incorporating MeNP of good electronic communication between the electrode substrate and the proteins, is seen by voltammetric techniques. This electronic wiring of proteins is a general advantage of using nanomaterials in LbL structures, exemplified by CNT/graphene LbL biosensors, reviewed in [44]. It was also observed at Au/AuNP/fullerenols-TvL modified electrodes, which displayed a pair of well-defined peaks with $E_m = 0.13$ V vs Ag/AgCl, attributed to the redox centre of the enzyme laccase,

in a diffusion-controlled electrochemical process. The increased k_s values compared to those obtained at TvL immobilized on an Au electrode without AuNP, was ascribed to electrode roughness and subsequent increased protein loading [21]. Even though the prosthetic group of Hb is deeply embedded in a protective protein, GCE/G/ZnO/AuNP/Hb exhibited the well-known pair of redox peaks attributed to the heme group in Hb. The peak height and reversibility increase in the order GCE/G/Hb < GCE/G/ ZnO/Hb < GCE/G/ZnO/AuNP/Hb [16]. Similarly, CNT-PtNP enabled direct electron transfer between the GOx redox centre and the GCE in GCE/chit$^+$(CNT-PtNP)/{conA/GOx}$_3$. CV at the GOx biosensor GCE/chit$^+$(CNT-PtNP)/{conA/GOx}$_3$ exhibited a pair of well-defined peaks, corresponding to the quasi-reversible redox process of the FAD cofactor inside GOx, with E_m = –0.42 V vs. SCE. Above 3 bilayers of Con A/GOx, the peak current decreased, since more layers of the film assembly increase the electron transfer resistance [31]. Heme redox peaks were increased at GCE/AuNP_C/Hb/Nafion compared to GCE/Hb/Nafion, and the high apparent electron transfer rate constant (k_s) of 2.64 s^{-1}, indicates a faster and more effective direct electron transfer between the immobilized Hb and the electrode. Moreover, the surface concentration of electroactive Hb was about 11 times that of the theoretical monolayer coverage of Hb, suggesting that AuNP_C offered a suitable matrix for Hb loading [6]. In [18], in order to realize good electronic communication between GOx and the electrode, the size of AuNP initially deposited needed to be increased, the cofactor peak at –0.41 V vs Ag/AgCl appearing only after the enlargement of NP [18]. This was also the case in [34], where AuNP were biocatalytically enlarged by the H_2O_2 generated in the enzymatic reaction, which acted as reducing agent to reduce $AuCl_4^-$ on the AuNP surface. The H_2O_2 oxidation current increased linearly with AuNP dimensions.

Communication between HRP and the electrode substrate was possible only after incorporating AuNP in the electrode architecture, cyclic bisureas providing a favourable micro-environment for the active immobilization of HRP [20].

In other cases, the presence of MeNP is crucial for an increase of the analyte response and/or induced catalytic effects. This was observed for H_2O_2 detection at different electrode architecures, e.g. GCE$^-$/{CNT-NH$^+_3$/(G/TiO$_2$-Pd)$^-$}$_9$ [24], FTO/PEI$^-$/{BSA-G$^+$/AuNP} [40], GC/TiN_NP/IL-NH$_3^+$/catalase$^-$ biosensor [25], PdNP-thionine based electrode [26], ITO/{CNT-PSS$^-$/PDDA$^+$}$_6$/AgNP [12], for glucose detection at GCE-ATP-GNs-AuNP [17], cholesterol at cholesterol oxidase biosensor containing both Pt_PdNP and AuNP [35], and choline at Pt/MPTMOS(CNT-PDDA$^+$/ChOx$^-$) [15]. In the case of PtNP incorporated in ITO/{(PtNP-PAMAM/CNT)$^+$/GOx$^-$}$_3$ [27], and AuNP in Au/MPTMOS/AuNP/Tyrosinase [14], and in GCE/CNT/ZnO/AuNP [41], the MeNP also caused an electrocatalytic effect. Similarly, PtNP loading up to 20% leads to a positive shift in the H_2O_2 reduction potential from –250 mV to 60 mV [33] and densely packed AgNP with smaller size were favourable for the electrocatalytic detection of H_2O_2 [12].

5. Applications of LbL biosensors based on metal nanoparticles

5.1. Electrochemical biosensors

Biosensor platforms containing metal nanoparticles, based on the self-assembling methodology, have been applied to the determination of a number of analytes, e.g. glucose, hydrogen peroxide (the key analyte in the enzymatic mechanism of many oxidases), cholesterol, cholines, lactate, pesticides, catechol, gallic acid and nitrite ions. DNA/RNA biosensors will also be included and the development of non-enzymatic LbL sensors for future biosensor applications, will also be briefly discussed. Applications since 2010 are summarised in Table 1.

5.1.1. Glucose biosensors

Seven glucose oxidase biosensors have been developed [17,18,24,27,31,33,34], among which two have applicability in the fuel cell area [17,27]. The majority make use, beside the MeNP, of carbon nanomaterials, such as CNT, graphene nanosheets (GNs) or carbon mesoporous materials (CMM), which used by themselves in LbL structures led to the development of efficient biosensors [44].

Table 1
Electrochemical biosensors based on MeNP and LbL methodology

Biosensor architecture	Analyte	Procedure	Sensitivity /μA cm^{-2} mM^{-1}	Linear range / mM	K_m / mM	LoD / μM	Ref
Au/{GOx_Cys_SP1/AuNP}$_4$	glucose	CV +0.5 V[2]	23.5	-80	-		[18]
GCE/chit$^+$(TiO$_2$_CNT)/PB$^-$/PDDA$^+$_AuNP/GOx$^-$		Amp. -0.1 V[1], pH 6.0	66.3	0.006-1.2	-	2	[34]
GCE/PDDA$^+$(CMM_PtNP)/GOx		FIA, amp. -0.2 V[1], pH 7.4	0.9	-0.05		2.5	[33]
GCE/chit$^+$(CNT_PtNP)/{conA/GOx}$_3$		Amp. +0.3 V[1], pH 7.0	41.9	0.001-2.0	0.64	0.4	[31]
GCE$^-$/{CNT-NH$_3^+$/(G/TiO$_2$–PdNP)$^-$}$_n$/ CNT-NH$_3^+$/GOx$^-$/Nafion		Amp. -0.05 V[1], pH 7.4	0.2	0.001-1.5	0.6	0.6	[24]
GCE/ATP/GNs_AuNP/GOx		CV -0.6 V[2], pH 7.4	47.6	1.0–12.0	-	9.3	[17]
GCE/G/ZnO/AuNP/Hb	H_2O_2	Amp. -0.3 V[1], pH 7.0	211.3	0.006-1.1	0.17	0.8	[16]
GCE/AuNP_C/Hb/Nafion		Amp. -0.4 V[1], pH 7.0	398	0.001-0.1	0.21	0.93	[6]
GCE/chit$^+$/{Fe$_3$O$_4$@PtNP$^-$/Hb$^+$}$_4$		Amp. -0.4 V[1], pH 7	11.9e[3]	0.001-0.2		0.03	[32]
ITO/MPTMOS(AuNP)/HRP		CV -0.5 V[1], pH 7.4	1.3*	-2.8	-	2.8	[13]
Au/MPA/CBU_AuNP/HRP		Amp. -0.3 V[1], pH 7.4	55e[3]*	0.4-0.9	4.5	0.05	[20]
GCE/TiN_NP/{IL-NH$_3^+$/catalase$^-$}$_7$		Amp. -0.35 V[2], pH 7.0	380	0.001-2.1	1.1	0.1	[25]
Au/MPS$^-$/PAH$^+$/PSS$^-$/{PAH$^+$(CNT_AuNP)/HRP$^-$}$_4$/ {PAH$^+$(CNT_AuNP)/ChlsOx$^-$}$_4$	cholesterol	Amp. -0.15 V[1], pH 7.0	12.3	0.18–11.0		20	[37]
GCE/PDDA$^+$(TiO$_2$–G)/Pt_PdNP$^-$/ PDDA$^+$(TiO$_2$–G)/AuNP$^-$/ChlsOx$^+$		Amp. -0.35 V[1], pH 7.0	1327	-0.6	0.21	0.017	[35]
Pt/MPTMOS(CNT_PDDA$^+$+ChOx+AuNP)/ {PDDA$^+$/AChE$^-$}$_2$	acetylcholine	Amp. +0.35 V[2], pH 7.0	3.4*	0.005-0.4	-	1.0	[15]
SPCE/MnO$_2$_NP/{PDDA$^+$/PAS$^-$}$_2$/{PDDA$^+$/ChOx$^-$}$_3$	choline	Amp. +0.5[2], pH 7.5	59.0	0.3–100	-	0.1	[38]
GCE/PDDA$^+$(CMM_PtNP)/LOx	L-lactate	FIA, amp. -0.2 V[1], pH 7.4	2.4	-0.05		1.7	[33]
GCE/CNT$^-$/(PAMAM-AuNP)$^+$/AChE$^-$	carbofuran	CV +0.63 V[1], pH 7.4		5e^{-6}–9e^{-5}	1.7	0.004	[28]
Au/MPTMOS/AuNP/tyrosinase	catechol	Amp. -0.18 V[2], pH 70	306.7	0.001-1.0		0.56	[14]
Au/cysteamine/AuNP-COOH/Fullerenols/TvL	gallic acid	FIA, amp -0.1 V[2], pH 4.5	42.7	0.03-0.3	0.66	6.5	[21]
GCE/chit$^+$/{Fe$_3$O$_4$@PtNP$^-$/Hb$^+$}$_n$	NO_2^-	Amp. -0.7 V[1], pH 5	8.7	0.002-0.1		0.3	[32]

[1] vs SCE; [2] vs Ag/AgCl; * area not specified.
Cys – cysteine, SP1 - stable protein 1, chit – chitosan, PB – Prussian blue, PDDA – poly(diallyl dimethylammonium) chloride, GOx – glucose oxidase, CMM – carbon mesoporous material, con A – concanavalin A, G – graphene, ATP - 4-aminothiophenol, GNs – graphene nanosheets, Hb – hemoglobin, MPTMOS – (3-mercaptopropyl)-trimethoxysilane, MPA – mercaptopropionic acid, CBU – cyclic bisureas, HRP – horseradish peroxidase, IL – ionic liquid, PAH – poly(allylamine hydrochloride), PSS$^-$ - polystyrene sulfonate, ChlsOx – cholesterol oxidase, ChOx – cholineoxidase, AChE – acetylcholineesterase, LOx – lactate oxidase, PAMAM – polyamidoamine, TvL – Trametes versicolor Laccase.

Stable protein 1 (SP1), was used to bind nanoparticles AuNP spontaneously with GOx to form two and three-dimensional structures. The new mutant, Au/{GOx_Cys_SP1/AuNP}$_4$ enabled direct communication between the FAD cofactor and the electrode substrate, the SWV revealing cofactor activity [18]. The system demonstrates the applicability of SP1 to assemble multiple enzyme units together with MeNP on a protein scaffold in a 3D model, with efficient electrical wiring by AuNP, for nanobioelectronic applications.

Prussian blue was used as redox mediator in a complex architecture comprising both CNT and AuNP, GCE/chit$^+$(TiO$_2$_CNT)/PB$^-$/PDDA$^+$-AuNP/GOx$^-$, at which the electrochemical process was diffusion controlled. The optimum pH between 4.5 and 8.0 was 6.0, while the response increased with more negative applied potential from+0.2––0.2 V vs SCE, –0.1 V being chosen with the aim to minimize interferences. The enzymatic mechanism was based on the reduction of H_2O_2 enzymatically generated at the PB mediator film, at potentials very close to 0.0 V vs SCE. The analytical applicability of the biosensor was evaluated by the standard addition method, the recovery rate for different glucose concentrations being between 94 and 104.4% [34].

Size-tunable Pt nanoparticles assembled on a mesoporous carbon were assembled as GCE/PDDA$^+$(CMM_PtNP)/GOx and GCE/PDDA$^+$(CMM_PtNP)/LOx and successfully used for the simultaneous on-line detection of glucose and L-lactate in brain microdialysate. The mesoporous carbon material (CMM) enabled the loading of different amounts of PtNP, and the architectures were tested by monitoring H_2O_2 reduction by linear sweep voltammetry which revealed that an increase in the PtNP loading from 5% to 10% increased the response to H_2O_2 and had an electrocatalytic effect, more than 20% bringing no further advantages. The use of a dual face GCE for an on-line selective simultaneous detection system, which minimizes possible cross-talk, enabled simultaneous monitoring of glucose and L-lactate. The dual biosensor was appropriate for the real-time determination of basal neurotransmitter levels in the extracellular brain space, being applied in "in vivo" experiments with on-line microdialysis system, for simultaneous detection of glucose and L-lactate in rat brain, with very good recovery rates [33].

Sugar–lectin biospecific interactions were used to form multilayer structures of Concanavalin A and GOx on a CNT_PtNP substrate, to obtain the glucose biosensor GCE/chit$^+$(CNT_PtNP){Con A/GOx}$_3$. Cofactor redox peaks appeared in cyclic voltammetry, in a surface-controlled electrochemical process [31].

Size-controllable PdNP assembled on TiO$_2$/graphene nanosheets (GNs) were used together with amino-terminated CNT for the fabrication of GCE$^-$/{CNT-NH$_3^+$/(G/TiO$_2$–PdNP)$^-$}$_n$/CNT-NH$_3^+$/GOx$^-$/Nafion. By comparing the performance of different GOx biosensors, it was observed that sensitivities increased in the order GCE GOx$^-$/Nafion < GCE/CNT-NH$_3^+$/GOx$^-$/Nafion < GCE$^-$/{CNT-NH$_3^+$/(G/TiO$_2$-Pd)$^-$}$_9$/GOx$^-$/Nafion. The biosensor has applicability for the "in vivo" determination of glucose in biological samples [24].

Two GOx biosensors were developed for fuel cell applications, one based on graphene nanosheets (GNs) and AuNP, GCE/ATP/GNs_AuNP/GOx [17] and one based on PtNP and CNT, ITO/{(PtNP-PAMAM/CNT)$^+$/GOx$^-$}$_n$ [27]. In [27] a Toray carbon paper coated with {(PtNP-PAMAM/CNT)$^+$/GOx$^-$}$_3$ served as anode and Pt electrodeposited on Toray carbon paper as cathode, the fuel cell having a power density of 17 μW cm^{-2} and a current density of 90 μA cm^{-2} [27].

Glucose biosensors maintained more than 84% of their initial response after 2 weeks of storage [24,33,34]; repeatability was determined to be more than 95% [24,31,33], and reproducibility 95% [31]. Negligible or no interferences were observed from glycine, L-cysteine [31,34], dopamine (DA) [24,33,34] ascorbic acid (AA) [24,31,33], uric acid [24,31], acetaminophen, dihydroxyphenylacetic acid and 5-hydroxytryptamine [33].

5.1.2. Hydrogen peroxide biosensors

Seven hydrogen peroxide biosensors were developed based on MeNP, the biorecognition elements being horseradish peroxidase (HRP) [13,19,20], hemoglobin (Hb) [6,16,32] and catalase [25]. All these electrode platforms, beside having the applicability for detecting H_2O_2 in samples of oils, plants, soil, milk, cream etc., have the potential to be applied to the construction of bi-enzymatic biosensors containing an oxidase enzyme in the upper layer, for which the enzymatic reaction by-product is H_2O_2, as exemplified by Au/MPS$^-$/PAH$^+$/PSS$^-$/{PAH$^+$(CNT_AuNP)/HRP$^-$}$_m$/{PAH$^+$(CNT_AuNP)/ChlsOx$^-$}$_n$ [37].

Horseradish peroxidase (HRP) is one of the most used enzymes in biosensor construction due to its biological role and, subsequently, its participation in various physiological processes. It is therefore extensively used in bi-enzyme biosensors, where H_2O_2, the by-product of an oxidase enzymatic reaction, is monitored. The use of MeNP and LbL methodology enables improved electronic communication between the enzyme and the electrode substrate. One of the studies was focused on determining the percentages of direct electron transfer (DET) and mediated electron transfer of HRP on a nanostructured substrate based on mercaptopyridine (MPy) self-assembled monolayer and AuNP decorated CNT (MPy/CNT_AuNP), since these types of nanomaterials are widely used as support for enzyme immobilization. Koutecky-Levich theory was used to obtain the kinetic current in the presence of H_2O_2 as well as H_2O_2 and dopamine, simultaneously. Comparison of the dependence of the kinetically limited currents on the peroxide concentration in the absence and presence of p-cresol (mediator) in solution shows that the DET increases from 51% in GCE/MPy(CNT)/HRP to 68% GCE/MPy(CNT+AuNP)/HRP, revealing the importance of AuNP [19].

A functional monolayer of 3-mercaptopropyltrimethoxysilane (MPTMOS) enabled the anchoring of HRP using specific chemical and physical interactions, and of AuNP ITO/MPTOS-AuNP$_{1,2}$/HRP [13], and similarly, one layer of mercaptopropionic acid (MPA) enabled the assembly of a cyclic bisurea_AuNP (CBU_AuNP) composite and the covalent attachment of HRP, to form Au/MPA/CBU_AuNP/HRP, which was then used for peroxide detection [20].

Apart from the usual redox enzymes used for H_2O_2 detection, HRP, cytochrome C, catalase, etc., Hb has recently often been used due to its commercial availability, relatively high stability and, most importantly, due to its intrinsic peroxidase-like activity [16,46]. Hemoglobin was immobilized onto a graphene, flower-like zinc oxide, and AuNP modified GCE, the GCE/G/ZnO/AuNP/Hb biosensor exhibiting an increase in the cathodic current at -0.8 V vs SCE upon H_2O_2 addition, no change in current being noted in the absence of Hb [16]. Gold nanoparticle-assembled capsules (AuNP_C) with controllable size and morphology, served to adsorb hemoglobin (Hb), to form GCE/AuNP_C/Hb/Nafion [6], and another H_2O_2 biosensor contained Hb immobilized together with core-shell nanoparticles of Fe_3O_4 covered by Pt (Fe_3O_4@PtNP) to form GCE/chit$^+$/{Fe_3O_4@PtNP$^-$/Hb$^+$}$_4$ [32]. The same biosensor was also used for the determination of $NO_2^{-\cdot}$ which generated a new reduction peak at about –0.7 V vs. SCE in CV, then being monitored by fixed potential amperometry [32].

The LbL assembly of catalase and amine-terminated ionic liquid onto titanium nitride nanoparticle modified GCE enabled the construction of a sensitive H_2O_2 biosensor, GCE/TiN_NP/{IL-NH$_3^+$/catalase$^-$}$_7$. The electrochemical process was surface controlled with a very high k_s of 5.3 s^{-1}, indicating fast electron transfer between the layers. The biosensor was successfully used to determine H_2O_2 in real samples, milk and bleaching cream [25].

Biosensors for H_2O_2 detection maintained 80% [20] and 94% [32] after 4 weeks, 94% after 3 [16], 96% [25] and 92% after 2 [6] and 100% [25] after 1 week of storage respectively. The RSD for different biosensors were less than 7% [16,20,32], with a repeatability of 95% [6,32].

5.1.3. Other enzyme biosensors

Two cholesterol oxidase (ChlsOx) biosensors were developed, one based on AuNP decorated CNT, Au/MPS$^-$/PAH$^+$/PSS$^-$/{PAH$^+$(CNT_AuNP)/HRP$^-$}$_m$/{PAH$^+$(CNT_AuNP)/ChlsOx$^-$}$_n$ [37] and the other on both TiO_2–G and AuNP, GCE/PDDA$^+$(TiO_2–G)/Pt_PdNP$^-$/PDDA$^+$(TiO_2–G)/AuNP$^-$/ChlsOx$^+$ [35]. The one based on CNT_AuNP, operated best at -0.15 V vs SCE, with no interferences from urea, glycine, l-cysteine, glucose, ascorbic acid [37], while the latter one had best performance at –0.35 V, also with lack of interferences from AA, UA, DA and glucose [35]. Both biosensors retained 90% of their initial activity after one month of storage at 4°C, with good reproducibility, the latter being applied to the determination of cholesterol in food samples, e.g. egg, meat, margarine and fish oil, in good agreement with the amount of the cholesterol listed on the product labels and determined by high performance liquid chromatography [35].

A novel acetylcholinesterase (AChE)/choline oxidase (ChOx) bienzyme amperometric acetylcholine biosensor based on AuNP and CNT, Pt/MPTMOS(CNT-PDDA$^+$+ChOx+AuNP)/{PDDA$^+$/AChE$^-$}$_2$, showed an increase in sensitivity up to two bilayers of PDDA$^+$/AChE$^-$. The biosensor amperometric response increased with applied potential from 0.1 to 0.35 V, remaining constant up to 0.7 V vs Ag/AgCl. The biosensor repeatability was of 95% with no interferences from AA, DA, UA, acetaminophen or serotonin and a good retention of initial activity of 80% after 2 months storage at 4°C. The concept has applicability for constructing multienzyme-based biosensors [15].

A choline biosensor was also developed based on MnO_2_NP, the enzyme being self-assembled with PDDA$^+$, SPCE/MnO_2_NP/{PDDA$^+$/PAS$^-$}$_2$/{PDDA$^+$/ChOx$^-$}$_3$, and used to analyse the activity of blood esterases, e.g. butyrylcholinesterase (BChE), detected in mice blood hemolysates with a LoD of 5 pM [38]. The same biosensor was used in the analysis of cholinesterase inhibitors for ecological monitoring and environmental surveillance, exemplified for chlopyrifos, the method with an LoD of 50 pM [38]. Similarly, the pesticide carbofuran was determined by inhibition measurements at AChE biosensor based on AuNP, i.e. GCE/{CNT$^-$/(PAMAM-AuNP)$^+$}$_n$/AChE$^-$. The biosensor retained 90% of its initial activity after 3 weeks of storage at 4°C, had a good precision of 95%, being applied for the determination of carbofuran in onion, lettuce and cabbage [28].

A tyrosinase biosensor based on AuNP, Au/MPTMOS/AuNP/tyrosinase, was used for the determination of catechol, monitored by cyclic voltammetry. In the absence of enzyme, no response from catechol was observed, while in the presence of both AuNP and enzyme, a reduction wave was observed, at -0.1 V vs Ag/AgCl. The biosensor had good repeatability with RSD = 3.5% and some small interferences from AA, acetaminophen and UA. The biosensor can be applied to the determination of phenolic compounds, which are important to be controlled due to their high toxicity and detrimental effects to human health [14]. Polyphenolic compounds, which include tannins and anthocyanins, can be determined in numerous samples, e.g. wine, coffee, tea, plant infusions, fruit/vegetable juice etc., by using the enzyme laccase. Two different nanostructured materials, AuNP and fullerenols, were used to develop a laccase biosensor based on Trametes versicolor Laccase (TvL) assembled in LbL structures on an Au electrode, Au/cysteamine/AuNP-COOH/fullerenols/TvL. The biosensor was used for the determination of the polyphenol index in two wines by flow injection analysis using fixed potential amperometry, with polyphenolic concentrations in agreement with those determined by the Folin-Ciocaltau method. The biosensor retained 87% of the initial sensitivity after 120 days [21].

5.1.4. Comparison between LbL and other enzyme biosensor platforms

From the research described above, there is strong evidence of the superior analytical properties exhibited by electrochemical enzyme biosensors containing MeNP and constructed by the self-assembly technique, in addition to the advantages of using metal nanoparticles, see Section 4. A glucose biosensor based on graphene/AuNP had lower detection limit and higher sensitivity [17], and the Hb based biosensor for H_2O_2 detection, based on same graphene/AuNP, exhibited better stability, higher linear range and lower detection limit [16]. An Fe_3O_4@PtNP/Hb biosensor, also for H_2O_2 detection, had similar stability and linear range, but lower detection limit, compared to other types of Hb biosensor [32]. In other cases, there is a clear increase in biosensor sensitivity on incorporating MeNP [13], or there is no response in their absence [18]. The Au/MPA/CBU_AuNP/HRP biosensor had a lower detection limit and K_m value compared with other HRP biosensors [20], while the immobilization of catalase with IL in LbL structures led to a biosensor with wider linear range, higher sensitivity and lower detection limit than more than 70% of the other catalase biosensors for H_2O_2 detection [25]. The incorporation of AuNP together with HRP and ChlsOx, led to a very reproducible device, with wider linear range [37], while the one based on the same enzyme in LbL structures with graphene and Pt_PdNP and AuNP had a lower K_m, wider linear range and lower detection limit [35], than other ChlsOx biosensors. A tyrosinase biosensor involving self-assembly of AuNP in a sol-gel matrix had a broader linear range than other tyrosinase biosensors for catechol detection [14].

5.1.5. Non-enzymatic architectures for biosensor development

Some LbL assemblies containing metal nanoparticles were developed and optimized for further employment as supports for biosensor construction, and are also presented in Table 1. Their catalytic properties are exemplified using common analytes, such as H_2O_2 [12,40] or nitrite [41], nitrophenol [7].

The catalytic properties of an electrode based on AgNP deposited on multilayers of CNT, was exemplified with H_2O_2 detection. The size and density of the AgNP influenced the sensor performance, smaller size and higher density of NP, the best being [12]. Another H_2O_2 sensor was based on AuNP, FTO/PEI$^-$/{BSA-G$^+$/AuNP}$_n$, its sensitivity being increased by a factor of 7 after thermal annealing, due to the removal of BSA [40].

The deposition of a ZnO layer enabled the deposition of smaller AuNP with no aggregation, which was beneficial in applying GCE/CNT/ZnO/AuNP to nitrite detection [41].

PS/PANI capsules used with adsorbed AuNP were used for the catalytic reduction of 4-nitrophenol, the dedoped PS/PANI@AuNP exhibiting the best catalytic activity, due to higher Au loadings, as well as stronger interaction between nitrogen-containing groups and AuNP [7].

5.1.6. DNA and RNA biosensors

LbL architectures have been developed for DNA biosensors, based on AuNP [22,47], Fe_3O_4_NP [23,39], and PtNP [36], an RNA biosensor based on PdNP [26] and an aptasensor for cocaine and thrombin detection, based on AuNP [42].

Visual detection of single-base mismatches (SBM) in DNA was possible by using a hairpin oligonucleotide with double-target DNA binding sequences and AuNP. The detection of SBM was based on the ability of hairpin oligonucleotide to distinguish between the perfect-matched DNA and SBM, generating different quantities of duplex DNA on the AuNP surface. This accumulation of AuNP produces the characteristic red bands, enabling visual detection of SBM [47].

AuNP were deposited on an ionic liquid modified carbon paste electrode, on top of which a layer of mercaptoacetic acid (MAA) was self-assembled, serving to cross-link the ssDNA. Methylene blue (MB) was the electrochemical indicator, being more strongly adsorbed on dsDNA than on ssDNA. A logarithmic dependence of the MB peak current with the concentration of Arabinose operon D gene target ssDNA sequence was obtained, with linearity in the concentration

range 10 pM–1 μM, and a detection limit of 1.5 pM. The precision of the biosensor was 97%, with 98.1% retention of initial response after 2 weeks of storage at 4°C. The biosensor was applied to detect the PCR product of Arabinose operon D gene sample extracted from arachis oil [22].

Magnetite nanoparticles (Fe_3O_4_NP) coated with cysteine were immobilized on SAM of mercaptobenzoic acid (MBA), and served as substrate for the immobilization of the DNA probe for tuberculosis. The hexacyanoferrate redox peak at Au/MBA/Fe_3O_4_NP/DNA, decreased with the increase in tuberculosis (Tb) genomic concentration. Similarly, the charge transfer resistance in electrochemical impedance spectra increased linearly with the increase of Tb DNA target concentration, up to 40 μg mL^{-1}, with a detection limit of 6 μg mL^{-1} [23].

Fe_3O_4_NP, PSS^- and $PDDA^+$ were self assembled together with HRP to get Fe_3O_4_NP/PSS^-/$PDDA^+$/HRP^-, on top of which AuNP/DNA were immobilized to give Fe_3O_4_NP-HRP/AuNP/DNA (FHAD) bioconjugates, used to amplify the signal to tetramethylbenzidine (TMB), a substrate for HRP. For this, an Au electrode was modified with the capture probe followed by hybridization with target DNA and subsequent hybridization with the receptor FHAD. The working principle was based on the oxidation of TMB by HRP in the hybridized bioconjugate, linearly proportional to the logarithm of target DNA concentration in the range 50 pM to 500 nM, with a detection limit of 7.1 pM. The selectivity was tested with two-base mismatched DNA and a non-complementary DNA, the biosensor showing no interferences. The RSD value was 8.4% (6 biosensors), with a 92% retention of initial activity after one week of storage at 4°C [39].

Based on a similar mechanism and involving TMB, negatively charged PtNP and CNT were self assembled through $PDDA^+$, and used to adsorb the DNAzyme, to get CNT^-/$PDDA^+$/$PtNP^-$/DNAzyme bioconjugate as trace tag for ultrasensitive sandwich DNA detection. The Au electrode was first modified with capture and target followed by hybridization with the DNAzyme bioconjugate, which is the receptor. DNAzyme, consists in hemin linked DNA and oxidizes TMB, the electroreduction of the enzymatically generated TMB, being amperometrically monitored. The amount of target DNA is directly related to the reduction charge of the TMB, and the currents of the DNA biosensor were logarithmically related to the target concentration in the range 1.0 fM to10 pM, with a detection limit of 0.6 fM. The selectivity was tested with non-complementary DNA and one-base mismatched DNA, no interferences being noticed [36].

An electrochemical microRNA biosensor using PdNP as enhancer and linker was developed comprising Nafion, thionine (TH) and PdNP, to obtain GCE/$Nafion^-$/TH^+/$PdNP^-$ used as substrate to immobilize the microRNA primer to detect target microRNA/155. The amount of H_2O_2 detected was inversely proportional to the amount of target microRNA/155, its hybridization leading to a decrease in the biosensor response to H_2O_2. The linear range was from 5.6 pM to 560 nM with a sensitivity of 1.73 μA pM^{-1} and a detection limit of 1.87 pM. The precision of the biosensor was close to 100%, with 90% retention of the initial response after 25 days of storage at 4°C. Its specificity for miRNA-155 detection was tested using two non-complementary sequences of thrombin aptamer and PDGF binding aptamer (PBA), with no interferences being observed [26].

An aptasensor for the detection of cocaine was developed based on ferrocene-appended poly(ethyleneimine) (Fc-PEI^+), $AuNP^-$ and cocaine aptamer fragments, SH-C2, to get ITO/PEI^+/PSS^-/{Fc-PEI^+/$AuNP^-$}$_2$/SH-C2. The ferrocene redox peaks decreased after assembling SH-C2, the addition of C_1 and cocaine leading to a further decrease in peak current, since SH-C2 hybridizes with C_1 to bind the cocaine to form SH-C_2/cocaine/C_1 complexes, which adsorb on the electrode surface, blocking the electron transfer process. Samples containing C1 and different concentrations of cocaine were incubated with the aptasensor and then the decreased DPV signal of the Fc was measured. The response of the aptasensor was linear in the concentration range 0.1–38.8 μM, with a RSD of 0.15 %, and a 96% initial response after 15 days storage at 4°C. The aptasensor was successfully applied to the determination of cocaine in biological fluids. The platform was also used for the detection of thrombin, by replacing the cocaine aptamer fragments, SH-C2, with thrombin aptamer segments, SH-TBA [42].

5.2. Optical (plasmonic) sensors

Surface plasmon resonance (SPR), which refers to the collective oscillations of the conduction electrons in metallic nanostructures, transduces a signal through shifts in the spectral position and intensity in response to external stimuli, normally in the visible range of the spectrum. SPR can also concentrate the incident electromagnetic field (EM) in a nanostructure, such that plasmon-enhanced fluorescence can be used for ultrasensitive detection. The refractive index sensitivity in SPR and localized SPR (LSPR) is strongly related to both intensity and decay length of the local EM field created at the resonance plasmon frequency, depending in turn on parameters including structure, geometry, material, surrounding environment [48]. MeNP, especially AuNP, have been extensively used as SPR sensors, and lately the use of the LbL technique has led to an increase in the sensitivity of such sensors, and has enabled the tailoring of the plasmonic properties of the MeNP-LbL optical sensors. Some examples are given here concerning the possibility to tailor the performance of optical sensors [49–52], with applications to the determination of anti-Rabbit IgG [49], lysozyme in human serum [50] and streptadivin [51,52].

UV–vis spectra of Au nanorods (AuNR) showed that an increase in the diameter and length following the deposition of each layer of negatively charged PSS^- and positively charged PAH^+ polyelectrolyte occurred, seen by a progressive red-shift and increase in the intensity of the longitudinal plasmon band. The rate of increase of EM decay length with nanorod diameter is significantly higher than that of the length, indicating that diameter can be used to tune the EM decay length of gold nanorods. This was exemplified by developing an antibody biosensor, in which a thiol-terminated polyethylene glycol (SH-PEG), served as flexible linker to increase the accessibility of IgG to get AuNR/SH-PEG/IgG, which, when exposed to goat anti-Rabbit IgG solution, resulted in a a red-shift in the LSPR wavelength of AuNR [49].

A self-assembled film of AuNP with a raspberry-like morphology was prepared by the LbL thermal annealing of multilayer films of negatively charged AuNP and PAH^+. The morphology and therefore the plasmonic properties of the films was controlled by changing the annealing temperature, duration of annealing, and number of layers. Above 300°C annealing temperature and for long annealing times, the raspberry-like morphology disappeared, and the LSPR sensitivity decreased. {$AuNP^-$/PAH^+}$_3$ film obtained after annealing at 300°C for 1 h functionalized with 11-mercaptoundecanoic acid (MUA) enabled the binding of lysozyme and a slight LSPR wavelength shift was observed for picomolar-range concentrations of lysozyme [50].

A three-dimensional gold nanoarchitecture was fabricated by LbL deposition of AuNP and CNT modified with 3-mercaptopropyltriethoxysilane (MPTES) so as to possess thiol groups, and was used in a plasmonic biosensor. The AuNP/CNT were modified with 11-amino-1-undecanethiol hydrochloride (11-AUT) and with EDC/NHS to be able to link biotin and streptavidin, used as model proteins for receptor-analyte binding experiments, or HSA and its antibody. A significant increase in the intensity of absorbance was observed upon incubation of biotin and HSA based biosensor upon incubation with streptavidin and the antibody, respectively [51].

An nm-thickness composite gold thin film consisting of negatively charged AuNP and PAH^+ was fabricated by using the LbL

technique. The reflection spectrum of a fibre probe as a function of number of coated $PAH^+/AuNP^-$ bilayers reveals that there is an increase in the intensity of the peak and an increase in its wavelength. To prove its efficiency, biotin was immobilized on $PAH^+/AuNP^-$ followed by the binding of streptavidin, which generated a wavelength red-shift of the peak, proportional to the streptavidin concentration [52].

6. Conclusions

The use of metal nanoparticles incorporated in self-assembled LbL architectures allows the development of well-organized biosensor architectures, leading to more efficient biosensor platforms with enhanced performance. The methodology used for MeNP synthesis influences their nanostructure, electrochemical and optical techniques allowing more control over the MeNP size and morphology. The incorporation of MeNP into self-assembled multilayers leads to an overall increase in electronic conductivity and electroactive surface area of the modified electrodes, enabling an improvement in the analytical performances of the corresponding biosensors. The biosensors developed since 2010 include 7 glucose biosensors based on GOx, 7 H_2O_2 biosensors, 3 based on Hb, 2 on HRP and 1 on catalase, 2 cholesterol biosensors both based on ChlsOx and 8 others for analytes such as acetylcholine, choline, carbofuran, L-Lactate, catechol, gallic acid and nitrite. Several biosensors based on nucleic acids DNA and RNA have been reported and showed the possible application of such devices in point-of-care diagnosis of genetic diseases as well as for detecting infectious agents or warning against bio-warfare agents. The use of MeNP in LbL architectures allowed the increase in sensitivity of optical sensors, also enabling exact control of the plasmonic properties of such devices, by varying MeNP size and distribution. The tailoring of nanomaterials such as metal nanoparticles in thin multilayers can bring further developments in the area of biosensors for their application in food/environmental industry, point-of-care diagnosis and fuel cells.

Acknowledgements

Financial support from Fundação para a Ciência e a Tecnologia (FCT), Portugal PTDC/QUI-QUI/116091/2009, POCH, POFC-QREN (co-financed by FSE and European Community FEDER funds through the program COMPETE and FCT project PEst-C/EME/UI0285/2013) is gratefully acknowledged. M.M.B. thanks FCT for postdoctoral fellowship SFRH/BPD/72656/2010.

References

[1] W. Zhao, J.-J. Xu, H.-Y. Chen, Electrochemical biosensors based on layer-by-layer assemblies, Electroanalysis 18 (2006) 1737–1748.
[2] J.J. Gooding, N. Darwish, The rise of self-assembled monolayers for fabricating electrochemical biosensors – an interfacial perspective, Chem. Rec. 12 (2012) 92–105.
[3] J.J. Gooding, S. Ciampi, The molecular level modification of surfaces: from self-assembled monolayers to complex molecular assemblies, Chem. Soc. Rev. 40 (2011) 2704–2718.
[4] G. Doria, J. Conde, B. Veigas, L. Giestas, C. Almeida, M. Assunção, et al., Noble metal nanoparticles for biosensing applications, Sensors 12 (2012) 1657–1687.
[5] M. Hasanzadeh, N. Shadjou, M. de la Guardia, Iron and iron-oxide magnetic nanoparticles as signal-amplification elements in electrochemical biosensing, TRAC Trend. Anal. Chem. 72 (2015) 1–9.
[6] J. Xuan, X.-D. Jia, L.-P. Jiang, E.S. Abdel-Halim, J.-J. Zhu, Gold nanoparticle-assembled capsules and their application as hydrogen peroxide biosensor based on hemoglobin, Bioelectrochemistry 84 (2012) 32–37.
[7] J. Yu, W.C. Guo, M. Yang, Y. Luan, J.Z. Tao, X.W. Zhang, Synthesis of hierarchical polystyrene/polyaniline@Au nanostructures of different surface states and studies of their catalytic properties, Sci. China Chem. 57 (2014) 1211–1217.
[8] K. Naka, Y. Chujo, Nanohybridized synthesis of metal nanoparticles and their organization, in: A. Muramatsu, T. Miyashita (Editors), Nanohybridization of Organic-Inorganic Materials, Springer, Berlin Heidelberg, 2009, pp. 3–40.
[9] P. Yu, Q. Qian, X. Wang, H. Cheng, T. Ohsaka, L. Mao, Potential-controllable green synthesis and deposition of metal nanoparticles with electrochemical method, J. Mater. Chem. 20 (2010) 5820–5822.
[10] R. Sato-Berrú, R. Redón, A. Vázquez-Olmos, J.M. Saniger, Silver nanoparticles synthesized by direct photoreduction of metal salts. Application in surface-enhanced Raman spectroscopy, J. Raman Spectrosc. 40 (2008) 376–380.
[11] I.V. Lightcap, T.H. Kosel, P.V. Kamat, Anchoring semiconductor and metal nanoparticles on a two-dimensional catalyst mat. Storing and shuttling electrons with reduced graphene oxide, Nano Lett. 10 (2010) 577–583.
[12] A. Yu, Q. Wang, J. Yong, P.J. Mahon, F. Malherbe, F. Wang, et al., Silver nanoparticle–carbon nanotube hybrid films: preparation and electrochemical sensing, Electrochim. Acta 74 (2012) 111–116.
[13] V. Ganesh, A. Muthurasu, Strategies for an enzyme immobilization on electrodes: structural and electrochemical characterizations, J. Phys. Conf. Ser. 358 (2012) 01200.
[14] X. Li, T. Ren, N. Wang, X. Ji, Gold nanoparticles-enhanced amperometric tyrosinase biosensor based on three-dimensional sol-gel film-modified gold electrodes, Anal. Sci. 29 (2013) 473–477.
[15] S. Hou, Z. Ou, Q. Chen, B. Wu, Amperometric acetylcholine biosensor based on self-assembly of gold nanoparticles and acetylcholinesterase on the sol–gel/multi-walled carbon nanotubes/choline oxidase composite-modified platinum electrode, Biosens. Bioelectron. 33 (2012) 44–49.
[16] L. Xie, Y. Xu, X. Cao, Hydrogen peroxide biosensor based on hemoglobin immobilized at graphene, flower-like zinc oxide, and gold nanoparticles nanocomposite modified glassy carbon electrode, Colloids Surf. B Biointerfaces 107 (2013) 245–250.
[17] R.K. Shervedani, A. Amini, Novel graphene-gold hybrid nanostructures constructed via sulfur modified graphene: preparation and characterization by surface and electrochemical techniques, Electrochim. Acta 121 (2014) 376–385.
[18] M. Frasconi, A. Heyman, I. Medalsy, D. Porath, F. Mazzei, O. Shoseyov, Wiring of redox enzymes on three dimensional self-assembled molecular scaffold, Langmuir 27 (2011) 12606–12613.
[19] S.M. Silva, D.M. Pimentel, R.C.S. Luz, F.S. Damos, Direct electron transfer kinetics of horseradish peroxidase on self-assembled monolayer/gold nanoparticles decorated multi-walled carbon nanotubes, Int. J. Electrochem. Sci. 7 (2012) 1348–1358.
[20] M. Mathew, N. Sandhyarani, A novel electrochemical sensor surface for the detection of hydrogen peroxide using cyclic bisureas/gold nanoparticle composite, Biosens. Bioelectron. 28 (2011) 210–215.
[21] C. Lanzellotto, G. Favero, M.L. Antonelli, C. Tortolini, S. Cannistraro, E. Coppari, et al., Nanostructured enzymatic biosensor based on fullerene and gold nanoparticles: preparation, characterization and analytic applications, Biosens. Bioelectron. 55 (2014) 430–437.
[22] H. Gao, X. Qi, Y. Chen, W. Sun, Electrochemical deoxyribonucleic acid biosensor based on the self-assembly film with nanogold decorated on ionic liquid modified carbon paste electrode, Anal. Chim. Acta 704 (2011) 133–138.
[23] M.P. Costa, C.A.S. Andrade, R.A. Montenegro, F.L. Melo, M.D.L. Oliveira, Self-assembled monolayers of mercaptobenzoic acid and magnetite nanoparticles as an efficient support for development of tuberculosis genosensor, J. Colloid Interface Sci. 433 (2014) 141–148.
[24] Y. Yu, Y. Yang, H. Gu, D. Yu, G. Shi, Size-controllable preparation of palladium nanoparticles assembled on TiO_2/graphene nanosheets and their electrocatalytic activity for glucose biosensing, Anal. Methods 5 (2013) 7049–7057.
[25] S. Saadati, A. Salimi, R. Hallaj, A. Rostami, Layer by layer assembly of catalase and amine-terminated ionic liquid onto titanium nitride nanoparticles modified glassy carbon electrode: study of direct voltammetry and bioelectrocatalytic activity, Anal. Chim. Acta 753 (2012) 32–41.
[26] X. Wu, Y. Chai, R. Yuan, H. Su, J. Han, A novel label-free electrochemical microRNA biossensor using Pd nanoparticles as enhancer and linker, Analyst 138 (2013) 1060–1066.
[27] J. Zhang, Y. Zhu, C. Chen, X. Yang, C. Li, Carbon nanotubes coated with platinum nanoparticles as anode of biofuel cell, Particuology 10 (2012) 450–455.
[28] Y. Qu, Q. Sun, F. Xiao, G. Shi, L. Jin, Layer-by-Layer self-assembled acetylcholinesterase/PAMAM-Au on CNTs modified electrode for sensing pesticides, Bioelectrochemistry 77 (2010) 139–144.
[29] M.M. Barsan, M. David, M. Florescu, L. Ţugulea, C.M.A. Brett, A new self-assembled layer-by-layer glucose biosensor based on chitosan biopolymer entrapped enzyme with nitrogen doped graphene, Bioelectrochemistry 99 (2014) 46–52.
[30] M. David, M.M. Barsan, M. Florescu, C.M.A. Brett, Acidic and basic functionalized carbon nanomaterials as electrical bridges in enzyme loaded chitosan/poly(styrene sulfonate) self-assembled layer-by-layer glucose biosensors, Electroanalysis 27 (2015) 2139–2149.
[31] W. Li, R. Yuan, Y. Chai, H. Zhong, Y. Wang, Study of the biosensor based on platinum nanoparticles supported on carbon nanotubes and sugar–lectin biospecific interactions for the determination of glucose, Electrochim. Acta 56 (2011) 4203–4208.
[32] C. Yu, Y. Wang, L. Wang, Z. Zhu, N. Bao, H. Gu, Nanostructured biosensors built with layer-by-layer electrostatic assembly of hemoglobin and Fe_3O_4@Pt nanoparticles, Colloids Surf. B Biointerfaces 103 (2013) 231–237.
[33] Y. Yu, Y. Yang, H. Gu, T. Zhou, G. Shi, Size-tunable Pt nanoparticles assembled on functionalized ordered mesoporous carbon for the simultaneous and on-line detection of glucose and L-lactate in brain microdialysate, Biosens. Bioelectron. 41 (2013) 511–518.

[34] M. Zhang, R. Yuan, Y. Chai, W. Li, H. Zhong, C. Wang, Glucose biosensor based on titanium dioxide-multiwall carbon nanotubes-chitosan composite and functionalized gold nanoparticles, Bioprocess Biosyst. Eng. 34 (2011) 1143–1150.
[35] S. Cao, L. Zhang, Y. Chai, R. Yuan, An integrated sensing system for detection of cholesterol based on TiO_2–graphene–Pt–Pd hybrid nanocomposites, Biosens. Bioelectron. 42 (2013) 532–538.
[36] X.-Y. Dong, X.-N. Mi, L. Zhang, T.-M. Liang, J.-J. Xu, H.-Y. Chen, DNAzyme-functionalized Pt nanoparticles/carbon nanotubes for amplified sandwich electrochemical DNA analysis, Biosens. Bioelectron. 38 (2012) 337–341.
[37] X. Cai, X. Gao, L. Wang, Q. Wu, X. Lin, A layer-by-layer assembled and carbon nanotubes/gold nanoparticles-based bienzyme biosensor for cholesterol detection, Sens. Actuators B Chem. 181 (2013) 575–583.
[38] E.A. Dontsova, Y.S. Zeifman, I.A. Budashov, A.V. Eremenko, S.L. Kalnov, I.N. Kurochkin, Screen-printed carbon electrode for choline based on MnO_2 nanoparticles and choline oxidase/polyelectrolyte layers, Sens. Actuators B Chem. 159 (2011) 261–270.
[39] X.-Y. Dong, X.-N. Mi, B. Wang, J.-J. Xu, H.-Y. Chen, Signal amplification for DNA detection based on the HRP-functionalized Fe_3O_4 nanoparticles, Talanta 84 (2011) 531–537.
[40] Q. Xi, X. Chen, D.G. Evans, W. Yang, Gold nanoparticle-embedded porous graphene thin films fabricated via layer-by-layer self-assembly and subsequent thermal annealing for electrochemical sensing, Langmuir 28 (2012) 9885–9892.
[41] A.-J. Lin, Y. Wen, L.-J. Zhang, B. Lu, Y. Li, Y.-Z. Jiao, et al., Layer-by-layer construction of multi-walled carbon nanotubes, zinc oxide, and gold nanoparticles integrated composite electrode for nitrite detection, Electrochim. Acta 56 (2011) 1030–1036.
[42] Y. Du, C. Chen, J. Yin, B. Li, M. Zhou, S. Dong, et al., Solid-state probe based electrochemical aptasensor for cocaine: a potentially convenient, sensitive, repeatable, and integrated sensing platform for drugs, Anal. Chem. 82 (2010) 1556–1563.
[43] S. Guo, E. Wang, Synthesis and electrochemical application of gold nanoparticles, Anal. Chim. Acta 598 (2007) 181–192.
[44] M.M. Barsan, C.M.A. Brett, Carbon nanomaterials in layer-by-layer structured electrochemical enzymatic biosensors, Stud. UBB Chem. LX 3 (2015) 31–52.
[45] M.M. Barsan, E.M. Pinto, C.M.A. Brett, Interaction between myoglobin and hyaluronic acid in layer-by-layer structures – an electrochemical study, Electrochim. Acta 55 (2010) 6358–6366.
[46] S. George, H.K. Lee, Direct electrochemistry and electrocatalysis of hemoglobin in nafion/carbon nanochip film on glassy carbon electrode, J. Phys. Chem. B 113 (2009) 15445–15454.
[47] Y. He, X. Zhang, S. Zhang, M.K.L. Kris, F.C. Man, A.-N. Kawde, et al., Visual detection of single-base mismatches in DNA using hairpin oligonucleotide with double-target DNA binding sequences and gold nanoparticles, Biosens. Bioelectron. 34 (2012) 37–43.
[48] M. Li, S.K. Cushing, N. Wu, Plasmon-enhanced optical sensors: a review, Analyst 140 (2015) 386–406.
[49] L. Tian, E. Chen, N. Gandra, A. Abbas, S. Singamaneni, Gold nanorods as plasmonic nanotransducers: distance-dependent refractive index sensitivity, Langmuir 28 (2012) 17435–17442.
[50] M. Inuta, R. Arakawa, H. Kawasaki, Use of thermally annealed multilayer gold nanoparticle films in combination analysis of localized surface plasmon resonance sensing and MALDI mass spectrometry, Analyst 136 (2011) 1167–1176.
[51] L. Guo, G. Chen, D.-H. Kim, Three-dimensionally assembled gold nanostructures for plasmonic biosensors, Anal. Chem. 82 (2010) 5147–5153.
[52] M. Wan, P. Luo, J. Jin, J. Xing, Z. Wang, S.T.C. Wong, Fabrication of localized surface plasmon resonance fiber probes using ionic self-assembled gold nanoparticles, Sensors 10 (2010) 6477–6487.